A reduced dimensionality quantum reactive scattering study of the insertion reaction O(1 D)+H2→OH+H

Jay K. Badenhoop, Hiroyasu Koizumi, and George C. Schatz

Citation: The Journal of Chemical Physics **91**, 142 (1989); doi: 10.1063/1.457502
View online: http://dx.doi.org/10.1063/1.457502
View Table of Contents: http://scitation.aip.org/content/aip/journal/jcp/91/1?ver=pdfcov
Published by the AIP Publishing

A reduced dimensionality quantum reactive scattering study of the insertion reaction $O(^1D)+H_2 \rightarrow OH+H$

Jay K. Badenhoop[a] and Hiroyasu Koizumi
Department of Chemistry, Northwestern University, Evanston, Illinois 60208-3113

George C. Schatz[b]
Joint Institute for Laboratory Astrophysics, University of Colorado and National Institute of Standards and Technology, Boulder, Colorado 80309-0440

(Received 3 February 1989; accepted 10 March 1989)

This paper presents a two degree of freedom model for describing the quantum dynamics of the insertion reaction $O(^1D) + H_2$ in which bend motions are treated with a sudden approximation. Comparison of product state vibrational distributions from a classical version of this model with three dimensional trajectory results indicates that the model is realistic. Quantum/classical comparisons for the model Hamiltonian indicate that recrossing is more important in the quantum dynamics, and as a result, the quantum reaction probability from ground state reagents is lower by as much as 40%. In addition, the quantum vibrational state distribution shows higher excitation than its classical counterpart. This difference in excitation is due to trajectories that produce vibrationally cold products, and it is found that these trajectories always cross the deepest part of the H_2O well.

I. INTRODUCTION

A major unsolved challenge in chemical dynamics is the quantum mechanical description of insertion reactions such as $O(^1D) + H_2 \rightarrow OH + H$. There are a number of reasons why such reactions have not been studied. The large number of states needed to describe the deep well that serves as an intermediate during reaction (H_2O is stable by >7 eV relative to $O(^1D) + H_2$) certainly provides a formidable obstacle to any sort of exact quantum treatment. In addition, neither approximate dynamical methods nor accurate quantum basis expansion calculations have yet to be implemented for reactions that have nonlinear reaction paths of the sort typically found for insertion reactions (where branching between two possible product channels is possible).

In this paper we present a two degree of freedom model for the quantum dynamical treatment of $O(^1D) + H_2$. This model is loosely based on previously developed reduced dimensionality[1] and reaction surface Hamiltonian[2] descriptions of chemical reactions, but in order to treat $O(^1D) + H_2$, it is necessary to introduce a new kind of bending sudden approximation that takes advantage of the abrupt increase in the H–O–H bending frequency that occurs during the insertion step. This approximation partitions a major amount of the energy available to the H_2O intermediate into bending energy, resulting in a much shallower effective well for the remaining stretch degrees of freedom. We will present evidence using trajectories that indicates that this way of partitioning energy is approximately correct but we should note from the outset that the model has several limitations, including (1) the assumption of infinite mass for the oxygen atom (which may limit applicability of the model to some kinds of insertion reactions), (2) inability to describe competition between insertion and abstraction reaction pathways, and (3) a very primitive description of the product rotational distributions. What the model should describe realistically are (1) product vibrational distributions, (2) recrossing effects, and (3) branching between OH and OD isotopes in the O + HD reaction. We will focus upon the first two of these quantities in this paper, making comparisons between quantum and classical treatments of the model in order to determine the importance of quantum effects. In addition we will compare our classical model results with a classical treatment of the full 3D dynamics in order to determine the reliability of the model.

The $O(^1D) + H_2$ dynamics has been the subject of a large number of 3D trajectory studies,[3–8] and in many respects these studies have been able to explain many features of the thermal and state resolved dynamics, but still there are a number of reasons for attempting a quantum study of this reaction. Classical trajectories have indicated in the past that the $O(^1D) + H_2$ reaction occurs predominantly by insertion, and this is probably still true despite a significant lowering of the abstraction barrier in recent *ab initio* calculations.[9] The insertion mechanism involves formation of a H_2O intermediate in a substantial fraction of collisions, which lasts for a few vibrational periods.[7] Given the tendency for classical dynamics to be more chaotic than quantum dynamics, and for quantum dynamics to be more sensitive than classical mechanics to exit channel adiabatic barriers, one suspects that there will be differences between the classical and quantum dynamical evolution of these complexes, especially for $O(^1D) + H_2$ with its two light hydrogen atoms. One difference that would be of interest is in the amount of recrossing of the entrance channel bottleneck back to reagents. Essentially nothing is known about quantum recrossing effects for reactions without potential barriers but if important it would be of major significance to the development of theories for determining thermal rate coefficients. It may also be that

[a] Present address: Department of Chemistry, University of Wisconsin, Madison, WI 53706.
[b] JILA Visiting Fellow, 1988–89. Permanent address: Department of Chemistry, Northwestern University, Evanston, IL 60208-3113. Author to whom correspondence should be addressed.

 0021-9606/89/130142-08$02.10

adiabatic barriers in the exit channel region will influence branching between direct and complex mechanisms, resulting in noticeable quantum effects on product state distributions and isotope branching ratios. In this context, it is interesting to note that the trajectory OH/OD branching ratio for $O(^1D)$ + HD[7] is still at odds with experiment.[10] Until recently it was unclear whether this problem might be due to the potential surface,[7] but recent *ab initio* calculations[9] suggest that the earlier surfaces of Schinke and Lester[4] are at least approximately correct, so it does not appear that improvements to these surfaces will change things much. One final reason for studying the quantum dynamics of $O(^1D)$ + H_2 is to characterize the density and lifetimes of resonance states, since such states may have measurable properties (spectra) that might be valuable for further experimental work. Recent studies of long lived metastable states of H_3^+ [11,12] provide an indication that the spectroscopy of highly excited molecules might be surprisingly simple, so it would be important to see what happens for H_2O.

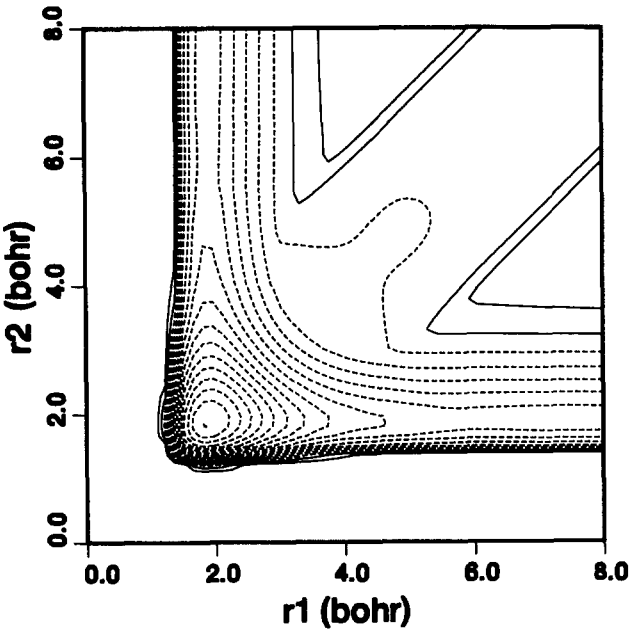

FIG. 1. Contours of V_m (derived from SL1 surface) versus r_1 and r_2 (both in a_0). Contours are in eV, with increments of 0.5 eV, and ranging from − 7.0 to 1.0 eV. Negative or zero energies relative to separated $O(^1D)$ + H_2 with H_2 at equilibrium are dashed contours; positive energies are solid contours.

II. THE DYNAMICAL MODEL

A. Coordinates for reaction surface

The reduced dimensionality methods of Refs. 1 and 2 provide general ways to define effective Hamiltonians for a given choice of coordinates that are to be actively treated. These coordinates clearly must describe the basic bond breaking and forming steps of the reaction, but there is much flexibility of choice of these coordinates within this framework. Unfortunately, past experience on reactions with collinear reaction paths[1,2] is not of much use for $O(^1D)$ + H_2. The choice we have made takes advantage of the great mass disparity that exists between O and H, which allows us to assume that the center of mass of the three atom system lies essentially on the O. In this case it is very natural to describe motions using the two OH distances r_1 and r_2, and the angle θ between them. r_1 and r_2 can be used to describe bond forming and breaking during reaction, so it is natural to choose r_1 and r_2 as the active coordinates and to eliminate θ. This separation has been used in the past to describe highly excited bound states of H_2O,[13] where θ motions tend to be slow compared to r_1 or r_2 motions, but to handle the complete reaction dynamics we also have to describe separated O + H_2 geometries where for certain orientations, θ motion corresponds to the fast H–H stretch, while r_1 and r_2 describe slow rotation.

Before we indicate how θ is to be removed, let us examine the potential surface as a function of r_1 and r_2. Clearly the most favorable "reaction surface" in these coordinates would involve minimizing the potential energy with respect to θ for each r_1 and r_2, and we denote such a minimized surface as $V_m(r_1,r_2)$. Choosing the often studied surface #1 of Schinke and Lester (SL1) to define the full dimensionality surface, the resulting plot of $V_m(r_1,r_2)$ is presented in Fig. 1. This surface has an easily recognizable H_2O well that is 7.1 eV below the reagents, the two equivalent OH + H product arrangement channels that are 2.2 eV below the reagents, and then the reagent arrangement channel that makes a 45° angle relative to the coordinates used for the plot. Since the minimum energy path for insertion involves no barrier in the perpendicular approach of O toward H_2, the surface has no barrier in the reagent channel region. Note that the $r_1 = r_2$ line corresponds to the H_2O symmetric stretch coordinate. In the separated O + H_2 region, motion perpendicular to this line (i.e., antisymmetric stretch motion) corresponds (for small displacements) to H_2 rotation. For larger displacements, when the H_2 has rotated to the point where the O–H_2 system is nearly linear, motion changes from rotation to H_2 stretching. In the region where antisymmetric stretch motion corresponds to rotation, the potential is independent of the antisymmetric stretch coordinate (provided that O and H_2 are sufficiently separated), and this produces the flat bottomed valley in Fig. 1. This is to be contrasted with the two OH + H valleys for which motion perpendicular to the bottom of the valley corresponds to OH vibration on a Morse-like potential.

B. Bending sudden approximation

In order to eliminate θ from the reaction dynamics we take advantage of the fact that the local bending frequency changes suddenly from a very high value (over 3500 cm^{-1}) in the reagent valley to a very low value (generally less than 500 cm^{-1}) elsewhere. Figure 2 shows a plot of this local harmonic bending frequency, which we have calculated using the following formula:

$$\omega_b = (k_b/I_b)^{1/2} \tag{1}$$

where

$$I_b^{-1} = 1/mr_1^2 + 1/mr_2^2. \tag{2}$$

Here k_b is the bend force constant and m is the H atom mass.

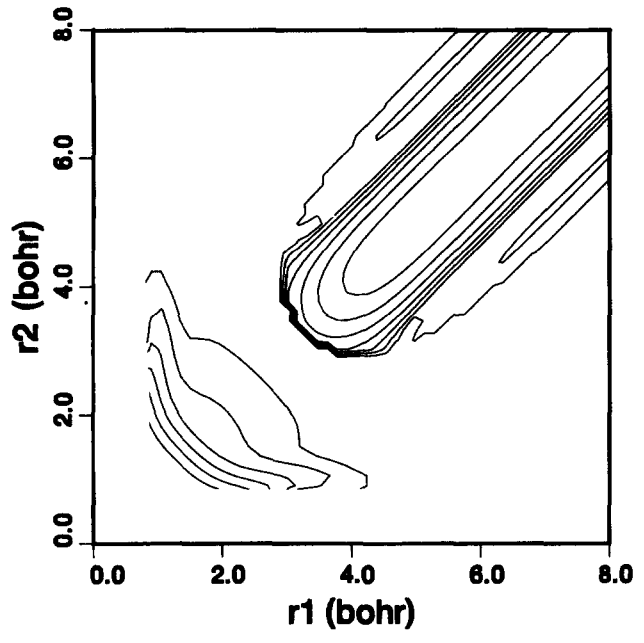

FIG. 2. Contours of the bend frequency (in cm^{-1}) versus r_1 and r_2. Contours are in increments of 500 cm^{-1}, starting at 500 cm^{-1}, with the highest contour (3500 cm^{-1}) enclosing a plateau in the upper right corner of the graph. Note that contours have been omitted for $r_1, r_2 < 0.8\ a_0$.

Equation (2) assumes an infinite oxygen atom mass, which we will use throughout this paper.

As we had anticipated, Fig. 2 shows that ω_b is high and relatively flat in the reagent valley, so we expect the reaction dynamics will be adiabatic relative to bending motion (which is really just H–H stretch motion) in this region. As we move down the $r_1 = r_2$ line towards H_2O equilibrium, ω_b drops suddenly at approximately $r_1 = r_2 = 3.35\ a_0$, to below 500 cm^{-1} over a distance of a few tenths of an atomic unit. A detailed analysis of the bending potential in this region reveals that the drop in bending frequency is sudden because it corresponds to a nearly discontinuous switch between one minimum at small H–H distances that is largely like the H–H stretch in separated O + H_2 and another at larger H–H distances that is largely like the bend potential of H_2O at equilibrium. At $r_1 = r_2$ values smaller than the switch region, ω_b drops to a minimum value, then rises up, passing through the H_2O equilibrium bend frequency (1568 cm^{-1} on the SL1 surface) near $r_1 = 1.8\ a_0$. As one moves out to the two product regions, ω_b goes to zero, for in this limit θ motion becomes OH rotation.

The sudden drop in bend frequencies near $r_1 = r_2 = 3.35\ a_0$ suggests that θ bending motion can be decoupled from r_1 and r_2 motion by using a sudden approximation. If we consider that initially we start in the O + H_2 arrangement channel, then the bend should remain adiabatic as we move down the symmetric stretch coordinate until $r_1 = r_2 = 3.35\ a_0$ is reached. The sudden approximation would involve projecting this initial adiabatic bend wave function onto bend wave functions associated with the much lower frequency H_2O bend motions that occur after the drop in frequency. If we imagine that r_1, r_2 motions are fast compared with θ motions after the drop in frequency (as makes sense given that the system is dropping into a well) then the bend wavefunction will remain unchanged from its form at $r_1 = r_2 = 3.35\ a_0$ as the system moves into the well, and the projection onto local bending states can be applied at any value of r_1 and r_2. The coefficients in this projection then determine how much energy is locked up into bend motions at that r_1, r_2. It is, however, inappropriate to apply the projection all the way into the product valleys, since the bend wave function by that point will have changed from its initial form. Thus we have to define an algorithm for switching off the sudden approximation as we move into the product regions. One way to do this is to apply the sudden approximation only along the $r_1 = r_2$ line. This determines a distribution of bending states at each value of the symmetric stretch coordinate, and this distribution can then be mapped away from the $r_1 = r_2$ line by taking advantage of the fact that the bend frequency varies slowly with respect to displacements of the antisymmetric stretch coordinate for $r_1, r_2 < 3.35\ a_0$. As a result, the bend distribution can be assumed to evolve adiabatically as a function of the antisymmetric stretch coordinate. This variation with antisymmetric stretch can be extended into the product valleys by using reaction path coordinates rather than normal coordinates, using the "path" that connects the H + OH and HO + H valleys. In this treatment, the bend distribution is taken to be invariant to motion along the reaction path for each value of the coordinate perpendicular to the reaction path.

To give a mathematical definition to what we mean, let us define $\Phi_n(\theta;r_1,r_2)$ as the adiabatic bend wave function in the O + H_2 valley associated with bend state n. This is parametrically a function of r_1 and r_2, and in the sudden approximation we use Φ_n evaluated at $r_1 = r_2 = r^*$ where r^* is just above the frequency drop. Next, define another group of bend states $\Psi_m(\theta;s,\rho)$ which are associated with the reaction path coordinates s (along the path, taking $s = 0$ at the $r_1 = r_2$ line) and ρ (perpendicular to the path). The sudden approximation involves projecting $\Phi_n(\theta;r^*,r^*)$ onto $\Psi_m(\theta,s,\rho)$ for $s = 0$ to determine the distribution of bend states at each ρ. The adiabatic part of this theory involves assuming that the distribution of bend states obtained at $s = 0$ is independent of s. From this distribution one can use the bend eigenvalues $\epsilon_m(s,\rho)$ to calculate the bend energy at each s and ρ. The sum of this and $V_m(r_1,r_2)$ then gives us a two dimensional potential $V_{\text{eff}}(r_1,r_2)$ upon which motion in r_1 and r_2 occurs. The specific fumctional form for V_{eff} is

$$V_{\text{eff}}(r_1,r_2) = V_m(r_1,r_2) + V_{\text{bend}}(r_1,r_2), \tag{3}$$

where

$$V_{\text{bend}} = \begin{cases} \epsilon_n(r_1,r_2) & r_1 > r^* \text{ and } r_2 > r^* \quad \text{(4a)} \\ \sum_m \epsilon_m[s(r_1,r_2),\rho(r_1,r_2)]\,|\langle \Phi_n(\theta;r^*,r^*)| \\ \quad \Psi_m[\theta,0,\rho(r_1,r_2)]\rangle|^2 & \\ & r_1 < r^* \text{ or } r_2 < r^* \quad \text{(4b)} \end{cases}$$

Equation (4a) defines the adiabatic bend energy in the reagent valley for a selected quantum number n, while Eq. (4b) defines the bend energy elsewhere in terms of the square of the projection coefficients at $s = 0$. Note that near

$r_1 = r_2 = r^*$, Φ and Ψ become identical and Eq. (4b) reduces to Eq. (4a).

One consequence of Eq. (4b) is that even in the product asymptotic regions there is still a nonzero bending potential as a function of the vibrational coordinate ρ. This acts very much like a centrifugal potential, as excited bends in this region are just OH rotations. However, the effective angular momentum in this potential varies with the vibrational coordinate, reflecting the fact that there really is a distribution of angular momentum values present. In fact one can use this feature to determine an OH rotational distribution by projecting the eigenfunctions of this effective OH vibrational potential onto the correct OH vibration/rotation eigenfunctions. Applying this to the SL1 surface leads to a most probable rotational quantum number for OH($v = 0$) of approximately $J = 25$, which is close to what one sees in trajectory calculations. The shape of this distribution is broader than what trajectories find, but the average rotational energy is accurate. Given the severe partitioning of energy between r_1,r_2 motions and bend motions that we are attempting, about the best that can be hoped for is getting the correct average split between bend and r_1,r_2 motions.

Fig. 3 plots contours of $V_{\text{eff}}(r_1,r_2)$ for the SL1 surface (taking the initial bend quantum number n to be zero). The bend eigenvalues and eigenfunctions used to generate this were obtained by using a simple finite difference code for a grid of r_1,r_2 values. To simplify the calculation, we replaced the bend distribution for each value of ρ by a Kronecker delta at the peak of this distribution. Figure 3 has the same general appearance as Fig. 1, but a key difference is in the depth of the H_2O well, which is only 2.2 eV relative to separated O + H_2. This shallower well compared to Fig. 1 reflects the fact that a major amount of energy is locked up in bending near the H_2O equilibrium. This makes scattering calculations feasible as we now discuss.

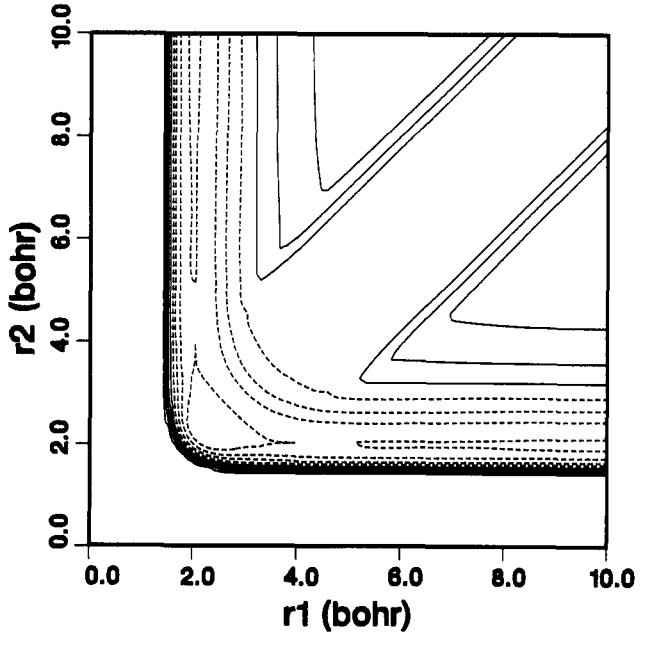

FIG. 3. Contours of V_{eff} versus r_1 and r_2. Contours are in increments of 0.5 eV starting at -2.0 eV.

C. Reactive scattering calculations

With the assumption of infinite oxygen atom mass, zero total angular momentum, and removal of the bend part of the problem into an effective potential V_{eff}, the Hamiltonian describing motions in the remaining coordinates r_1 and r_2 is

$$H_{\text{eff}} = -\frac{\hbar^2}{2m}\left(\frac{1}{r_1}\frac{\partial^2}{\partial r_1^2}r_1 + \frac{1}{r_2}\frac{\partial^2}{\partial r_2^2}r_2\right) + V_{\text{eff}}(r_1,r_2). \quad (5)$$

The radial kinetic energy terms can be simplified in the usual way[14] leading to

$$H_{\text{eff}} = -\frac{\hbar^2}{2m}\left(\frac{\partial^2}{\partial r_1^2} + \frac{\partial^2}{\partial r_2^2}\right) + V_{\text{eff}}(r_1,r_2). \quad (6)$$

This Hamiltonian describes motions of a single mass point on the potential surface in Fig. 3, and in this respect the structure of the problem is very much like that of a collinear atom–diatom reaction except that all three asymptotic arrangement channels are present.

To determine scattering wave functions for this problem we have developed a new kind of reactive scattering program based on hyperspherical coordinates in which the asymptotic boundary conditions are defined relative to three (rather than the usual two) arrangement channels. In this program we introduce the usual[15] hyperspherical radial (ζ) and angular (η) coordinates via

$$\zeta = (r_1^2 + r_2^2)^{1/2}, \quad (6a)$$

$$\eta = \tan^{-1}(r_2/r_1). \quad (6b)$$

The radial part of the problem is then divided up into sectors that range from a minimum ζ value (ζ_{min}) where the wave function can be assumed to be zero to a maximum ζ value (ζ_{max}) where the wave function will have "trifurcated" into the three asymptotic arrangement channels. Within each sector we then define η dependent basis functions by solving the one-dimensional Schrödinger equation for η motions within that region using a finite difference method. Expanding the wave function in that basis, we then convert the complete Schrödinger equation into coupled channel equations which are then solved by standard methods.[16]

At $\zeta = \zeta_{\text{max}}$ we project the scattered wave functions onto asymptotic coordinate basis functions that are localized in each of the three asymptotic arrangement channels. This involves determining the scattering wave functions in a small range of ζ which overlaps with three appropriately chosen straight line segments in Fig. 3 that correspond to constant values of the asymptotic translational coordinates. The scattering wave functions are then projected onto asymptotic basis functions, defining initial conditions for separate coupled channel propagations in each arrangement channel. When the potential becomes asymptotic, the scattering solutions are matched to incoming and outgoing waves to determine the scattering and probability matrices. The mathematical description of all these steps involves straight forward adaptation of earlier work[14,16,17] to the three arrangement channel problem so we will not repeat it.

In application to $O(^1D)$ + H_2, we found that converged reaction probabilities could be obtained using a basis of 39 hyperspherical basis functions which get divided into 13 functions in each OH + H arrangement channel and 13

in the O + H_2 channel. These numbers can, of course, be reduced by taking advantage of the intrinsic symmetry of the effective potential.

D. Quasiclassical trajectory calculations

In order to study quantum effects, and to calibrate our model results with 3D trajectory calculations, we have developed a quasiclassical trajectory method for our two degree of freedom model. Normally the technology of two degree of freedom trajectory calculations is rather standard,[18] but in the present application, the calculation of quasiclassical initial conditions for the potential in Fig. 3 is somewhat tricky. It turns out that although the potential energy V_m plotted in Fig.1 is initially flat and then increases with increasing antisymmetric stretch coordinate for separated O + H_2 (as explained in Sec. II A), the bend energy V_{bend} decreases with increasing $|s|$, and the sum V_{eff} has a symmetric double well as a function of s. This is not apparent in Fig. 3 since the two wells are rather shallow (0.22 eV deep) but they are deep enough to support two bound states below the barrier top which correspond to the ground and first excited rotational states of H_2. Physically what this corresponds to is a small preference in the absence of potential anisotropy for the O–H_2 system to be close to linear as a result of adiabatic bend energy differences that arise from the shape dependent factor in Eq. (2). These wells persist even asymptotically in our model because the bend and stretch coordinates that we are using have been imprecisely uncoupled in this region.

In the quantum eigenfunctions of this double well there is some tunneling through the barrier so the two solutions below the barrier top are split in energy by a small amount, with the lowest being at $E = 0.196$ eV [relative to separated $O(^1D)$ + H_2 with H_2 at its classical equilibrium] and the other at 0.201 eV. (The barrier top in these units is at 0.260 eV.) Our quasiclassical treatment has only considered the primitive semiclassical approximation to this double well, with tunnelling neglected, so the energies of both states are the same and equal to 0.197 eV. This by itself is not of major importance, but what is important is the fact that in the quantum description these two functions are, respectively, even and odd with respect to reflection ($s \rightarrow -s$, or equivalently, interchange of the two hydrogen atoms) and this makes the reaction dynamics starting from these states very different, while in the quasiclassical description such phase information is not used, and the dynamics from each state is the same. We shall see below that the effect of symmetry is to restrict what regions of the potential energy surface are sampled during collisions, and this leads to notable differences between the amount of quantum and classical recrossing of the entrance channel bottleneck and in the product vibrational distributions.

The quasiclassical calculations were done using 200 trajectories at each energy, uniformly sampling the phase angle associated with oscillation in the reagent double well. This phase angle as well as the reagent and product vibrational actions were defined numerically since the potential functions involved could not be described by simple analytical functions.

III. RESULTS

A. Product vibrational distributions

1. Comparison of 3D and reduced dimensionality trajectory results

To assess the accuracy of the assumptions involved in the model, let us begin by comparing 3D trajectory OH product vibrational distributions with those from quasiclassical calculations done using the reduced dimensional model. Figure 4 presents these distributions as a function of the OH quantum number v' at a total energy E of 0.40 eV, including (a) 3D trajectory results with the correct oxygen atom mass and with full sampling of impact parameters, (b) 3D trajectory results for correct oxygen mass and zero impact parameter b (also zero total angular momentum since the initial H_2 has $v = j = 0$), (c) 3D trajectory results for $b = 0$ and infinite oxygen atom mass, and (d) reduced dimensionality results. The 3D and model reagent zero point energies differ by about 0.07 eV, so the reduced dimensionality distributions were generated using a total energy of 0.33 eV so that the initial translational energy would be the same as in the 3D calculations. In addition, the reduced dimensionality distributions show strong variation with energy at certain special energies so we have smoothed this out by averaging over a 0.01 eV window centered at 0.33 eV to produce the results in Fig. 4. (This averaging actually has little effect at 0.33 eV, but is somewhat more important in the lower energy results that will be presented later.)

The curve (a) results in Fig. 4 agree within statistical uncertainty with equivalent results from Schinke and Lester[4] at approximately the same energy. This curve is nearly flat between $v' = 0$ and 4 and then drops to essentially zero at $v' = 6$. This is also in rough agreement with experiment,[19] although the experimental distribution drops off more quickly at high v' because the reaction exoergicity is too high on the *ab initio* SL1 surface compared to experiment and the OH vibrational frequency is too small.

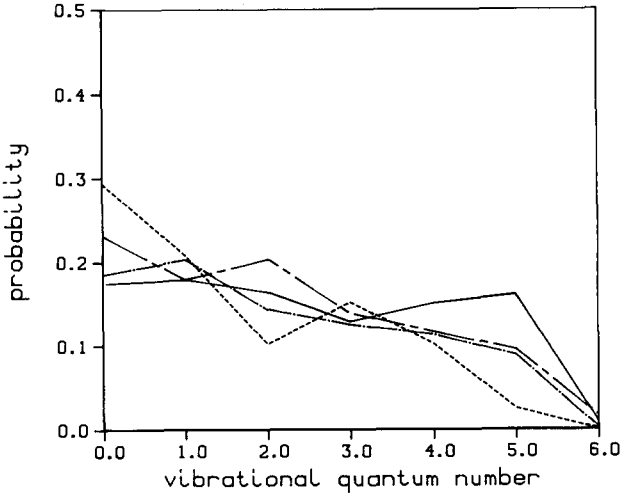

FIG. 4. Quasiclassical product OH vibrational distributions (normalized to sum to unity) at $E = 0.40$ eV as follows: (a) 3D, finite oxygen atom mass, sampling all impact parameters (long dash–short dash curve), (b) 3D, finite oxygen mass, $b = 0$ (solid curve), (c) 3D, infinite oxygen mass, $b = 0$ (dash–dot curve), (d) reduced dimensionality model (short dash curve).

Comparing curves (a) through (c), we see that the assumptions of zero impact parameter and infinite oxygen atom mass have essentially no influence on the product vibrational distributions, with all three curves in close agreement. Curve (d) is not in quite as good agreement with the other three, with a more noticeable bimodel shape, and a slightly earlier drop-off at high v', but the coarse-grained appearance is reasonably close to the other curves.

2. Comparison of classical and quantum results for reduced dimensionality model

Figure 5 presents a comparison of the $v = 0$ classical and quantum vibrational distributions at $E = 0.219$ and $E = 0.290$ eV for our reduced dimensionality model. For both classical and quantum distributions, we have averaged over the initial states $j = 0$ and 1 so as to minimize the effect of even/odd symmetry differences on the quantum distributions as was noted in Sec. II D. We will consider distributions for individual j states in Sec. III B 2. The two energies considered in Fig. 5 were chosen because the quantum probabilities do not show important resonance effects at these energies, and they are close to the lower and upper energies for which classical/quantum comparisons are possible with just two initial states being open.

$E = 0.219$ eV is just slightly above the classical threshold for reaction in our model, but the distributions at both energies are similar, with the classical distributions peaked at low v' (0 for 0.219 eV and 1 for 0.290 eV), while the quantum distributions are peaked at higher v' ($v' = 2$ at 0.219 eV and $v' = 3$ at 0.290 eV). The 0.219 eV quantum distribution also shows a peak at $v' = 0$, but it is much smaller than the corresponding classical peak. Despite these differences, at both energies the classical and quantum results agree well in the high v' drop off. This suggests that whatever mechanism is responsible for the high v' tail, it operates the same way in both classical and quantal descriptions.

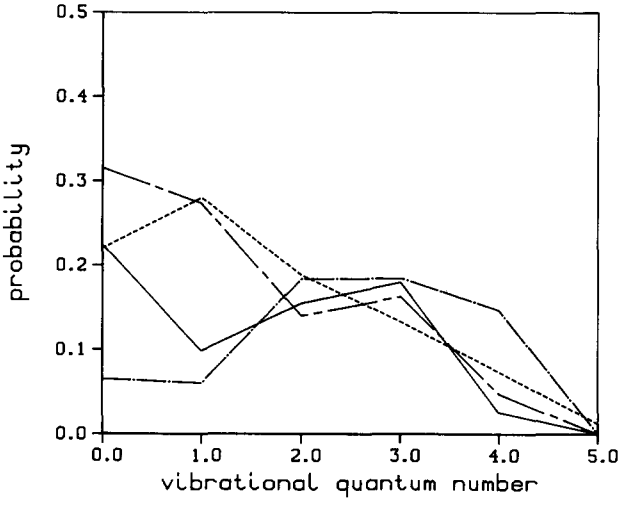

FIG. 5. Reduced dimensionality quasiclassical and quantum reaction probabilities for $v = j = 0$ versus OH vibrational quantum number v' at $E = 0.219$ and 0.290 eV. Curves are labelled as follows: quantum at 0.219 eV (solid curve), quantum at 0.290 eV (dash–dot curve), quasiclassical at 0.219 eV (long dash-short dash), quasiclassical at 0.290 eV (short dash).

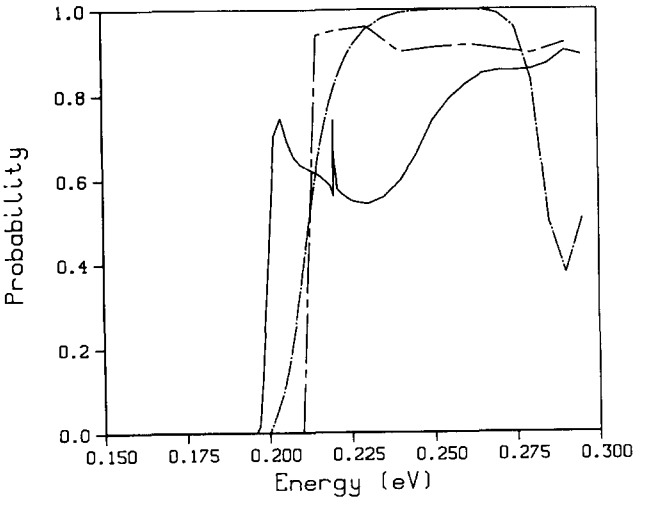

FIG. 6. Quasiclassical and quantum probabilities for $v = 0$, $j = 0$ and 1, summed over v', versus E. Curves are labeled as follows: quantum $j = 0$ (solid curve), quantum $j = 1$ (dash–dot), quasiclassical $j = 0$ or 1 (long dash–short dash).

To further explore the differences between classical and quantal pictures we have examined plots of the trajectories, and find that distinctly different trajectories are responsible for the high and low v' parts of the distributions in Fig. 5. The high v' tail is produced by trajectories that avoid the deepest part of the H_2O well, while low v' comes from trajectories that pass through the deepest part of the H_2O well, bouncing near the "corner" of the potential in Fig. 3. Neither type of trajectory involves long lived complexes, although there are often 2–3 bounces in or around the H_2O well. The comparison of classical and quantum results in Fig. 5 suggests that reactive trajectories which hit the corner of the potential are in some sense deemphasized in the quantum dynamics.

B. Energy dependence of reaction probabilities

1. Probabilities summed over final states

Now consider Fig. 6 where we plot the reaction probability for $v = 0, j = 0$ and 1 versus E for both the classical and quantal results. Note from Sec. II D that the classical results for both states are the same, and that there is a small barrier to reaction that shifts the classical threshold up to 0.215 eV (compared to quantum energetic thresholds of 0.196 and 0.201 eV for $j = 0$ and 1, respectively).

Figure 6 shows that both quantum probabilities rise fairly quickly from their energetic thresholds, with the $j = 1$ curve shifted up in energy by about 0.015 eV from $j = 0$. (This shift is by accident the correct rotational energy splitting between $j = 0$ and $j = 1$ in isolated H_2.) In contrast to the classical probability which rises to about 0.95 and is relatively constant, the quantum probabilities plateau at different values and have a more complex energy dependence. The $j = 0$ curve is especially interesting, for in this case the probability is roughly equal to 0.6 between 0.20 and 0.25 eV and then rises to about 0.85 at higher E. In addition, there is a sharp resonance-like feature at 0.220 eV. The $j = 1$ curve rises more slowly than $j = 0$ and has a plateau at 1.0, followed by a broad dip at 0.28–0.29 eV.

One important conclusion to be derived from Fig. 6 concerns *recrossing*. In the classical description of the problem, recrossing refers to trajectories that return to the reagents after first crossing some sort of reagent bottleneck. In the present model this bottleneck is well defined because of the small entrance channel barrier. An analysis of the trajectories indicates that all trajectories above 0.215 eV initially cross this bottleneck, which means that the small deviation between the reaction probability and unity (5%) represents recrossing. In the quantum results we have not separated our probabilities into contributions from reflection before the barrier and from recrossing, but it seems reasonable to assume that the probability plateau represents the effect of recrossing. What we see then is that recrossing is significant for $j=0$, representing 40% of the probability at low energy, while it is unimportant for $j=1$. The difference between $j=0$ and $j=1$ presumably reflects the symmetry properties of the wave function. $j=0$ is symmetric with respect to interchange of the H atoms, so the system can scatter off the inner corner of the H_2O potential well while $j=1$ is antisymmetric, so the system tends to avoid the well region. Apparently some fraction of the $j=0$ quantum flux must bounce back to the reagent valley after hitting this inner corner, leading to the observed recrossing.

It is also important to note how smooth the quantum reaction probabilities are as a function of E, as this suggests mainly direct reactive scattering. There is a narrow resonance peak in the $j=0$ curve at $E=0.220$ eV, and there is a broad dip in the $j=1$ curve near 0.285 eV, but these do not represent the only resonant states possible in this system over the energy range studied. We have examined other scattering probabilities associated with our model Hamiltonian (such as the H + OH → OH + H reaction probabilities) and find substantial resonance structure in them even well below the O + H_2 threshold, but this structure does not show up in the probabilities in Fig. 6. The obvious conclusion from this is that the O + H_2 quantum reaction dynamics is predominantly direct.

2. State to state reaction probabilities

Now let us consider the vibrational distributions associated transitions starting from $j=0$ and 1 at selected energies. Table I presents results at $E=0.219$, 0.220, 0.250, and 0.290 eV. Note that the averages of the $j=0$ and 1 results at 0.219 and 0.290 eV are what are plotted in Fig. 5.

The two closely spaced energies 0.219 and 0.220 eV, were selected to show how the sharp resonance at 0.220 eV influences the $j=0$ vibrational distributions. What we see is that the $v'=0$ peak present at 0.219 eV in the $j=0$ probability disappears at 0.220 eV, while the $v'=3$ peak shifts to $v'=2$ and is broader and larger. A further increase in the energy (say to 0.221 eV) returns to distribution to what it is at 0.219 eV. At still higher energies such as 0.250 eV, the $j=0$ distribution shifts so as to emphasize the high v' peak relative to that at $v'=0$, and at 0.290 eV, the $v'=0$ peak is gone.

Considering now the $j=1$ probabilities, we find that they are all similar at 0.219, 0.220, and 0.250 eV, with a peak at $v'=2$ and a second peak at $v'=0$. At 0.290 eV, which is in the region of the dip in Fig. 6, the high v' peak shifts up to $v'=4$.

TABLE I. Quantum reaction probabilities for $O(^1D)+H_2(v=0,j) \rightarrow OH(v')+H$.

j	v'	$E=0.219$ eV	0.220 eV	0.250 eV	0.290 eV
0	0	0.266	0.010	0.107	0.033
	1	0.028	0.155	0.022	0.074
	2	0.048	0.300	0.241	0.354
	3	0.223	0.197	0.239	0.306
	4	0.016	0.089	0.132	0.134
1	0	0.183	0.194	0.284	0.097
	1	0.168	0.172	0.243	0.045
	2	0.263	0.274	0.296	0.014
	3	0.138	0.143	0.165	0.063
	4	0.034	0.032	0.009	0.158

It is interesting to note that the $j=0$ and $j=1$ vibrational distributions are generally quite different, with $j=0$ showing a very distinct high v' peak and a smaller $v'=0$ peak at most energies, while for $j=1$ the high v' and low v' peaks are strongly overlapped and generally involve less overall excitation.

IV. CONCLUSION

This paper has presented a simple two degree of freedom model for the $O(^1D)$ + H_2 insertion reaction which is based on a sudden approximation for describing the evolution of bending motions from reagents to products. While the model clearly has important limitations, comparisons of classical results using the model Hamiltonian with 3D trajectories indicates that it describes product state distributions realistically. Most of our analysis was centered on understanding quantum effects through comparisons of exact quantum and quasiclassical results for the model Hamiltonian. These comparisons indicate that quantum dynamics can exhibit much more recrossing than classical dynamics, which is a conclusion that has important consequences with respect to the use of either trajectories or transition state theory to calculate thermal rate coefficients for this reaction. In addition, we found that the trajectory vibrational distribution peaks at $v'=0$ or 1 at low energy while the corresponding quantum distribution peaks at $v'=2$ or 3, with sometimes a second peak at $v'=0$. An analysis of the trajectories indicated that those producing $v'=0$ or 1 always pass close the deepest part of the H_2O well while those producing $v' \geqslant 2$ avoid this region. This suggests that the reactive quantum flux must be avoiding the H_2O well region, and we might speculate here that flux hitting this region must be reflecting back to the reagents, leading to the enhanced quantum recrossing. One piece of evidence in favor of this idea is the absence of significant recrossing in the reaction probability out of the first excited state of the reagents ($j=1$). This state has a node passing through the H_2O equilibrium geometry and is thus constrained by symmetry to avoid regions of the the potential that might lead to efficient recrossing. The difference between the recrossing probability for $j=0$ and $j=1$ might be detectable experimentally by

comparing rate coefficients for the reaction of $O(^1D)$ with para and ortho hydrogen.

A number of further studies are suggested by this work, including studies of $O(^1D)$ + HD to see if the isotope ratio is sensitive to quantum effects, extensions of the model to include nonzero total angular momentum, and a detailed examination of reactive scattering resonances to determine what kinds of motion are involved, and how this influences their widths. Improvements to the bending sudden approximation would also be desirable, and a number of modifications can be imagined concerning the choice of coordinates and the mixing of adiabatic and sudden approximations that might lead to improvement over the present treatment.

ACKNOWLEDGMENT

This research was supported by NSF Grant No. CHE-8715581.

[1]J. M. Bowman, Adv. Chem. Phys. **61**, 115 (1985).
[2]T. Carrington and W. H. Miller, J. Chem. Phys. **81**, 3942 (1984); **84**, 4364 (1986).
[3](a) P. A. Whitlock, J. T. Muckerman, and P. M. Kroger, in *Potential Energy Surfaces and Dynamics Calculations*, edited by D. G. Truhlar (Plenum, New York, 1981), p. 551. (b) P. A. Whitlock, J. T. Muckerman, and E. R. Fisher, J. Chem. Phys. **76**, 4468 (1982).
[4]R. Schinke and W. A. Lester, J. Chem. Phys. **72**, 3754 (1980).
[5]L. J. Dunne and J. N. Murrell, Mol. Phys. **50**, 635 (1983).
[6]S. W. Ransome and J. S. Wright, J. Chem. Phys. **77**, 6346 (1982).
[7]M. S. Fitzcharles and G. C. Schatz, J. Phys. Chem. **90**, 3634 (1986).
[8]P. J. Kuntz, B. I. Niefer, and J. J. Sloan, J. Chem. Phys. **88**, 3629 (1988).
[9]S. P. Walch and L. B. Harding, J. Chem. Phys. **88**, 7653 (1988).
[10]K. Tsukiyama, B. Katz, and R. Bersohn, J. Chem. Phys. **83**, 2889 (1985).
[11]J. M. G. Llorente and E. Pollak, J. Chem. Phys. **89**, 1195 (1988).
[12]J. M. G. Llorente, J. Zakrzewski, H. S. Taylor, and K. C. Kulander, J. Chem. Phys. **89**, 5959 (1988).
[13]G. A. Natanson, G. S. Ezra, G. Delgado-Barrio, and R. S. Berry, J. Chem. Phys. **81**, 3400 (1984); **84**, 2035 (1986).
[14]G. C. Schatz and A. Kuppermann, J. Chem. Phys. **65**, 4642 (1976).
[15]J. A. Kaye and A. Kuppermann, Chem. Phys. Lett. **77**, 573 (1981); J. Manz and J. Römelt, *ibid.* **81**, 179 (1981); D. K. Bondi, J. N. L. Connor, J. Manz, and J. Römelt, Mol. Phys. **50**, 467 (1983).
[16]G. C. Schatz, Chem. Phys. Lett. **150**, 409 (1988)
[17]G. C. Schatz, L. M. Hubbard, P. S. Dardi, and W. H. Miller, J. Chem. Phys. **81**, 231 (1984).
[18]J. M. Bowman and A. Kupperman, Chem. Phys. Lett. **12**, 1 (1971).
[19] J. E. Butler, R. G. MacDonald, D. J. Donaldson, and J. J. Sloan, Chem. Phys. Lett. **95**, 183 (1983).